The contribution of Galactic TeV pulsar wind nebulae to Fermi-LAT diffuse emission

Vittoria Vecchiotti (vittoria.vecchiotti@gssi.it)
GSSI

Giulia Pagliaroli
GSSI

Francesco Villante
Università degli studi dell'Aquila

Article

Keywords: Pulsar Wind Nebulae, Galactic Cosmic Ray

Posted Date: May 25th, 2021

DOI: https://doi.org/10.21203/rs.3.rs-539249/v1

Version of Record: A version of this preprint was published at Communications Physics on June 24th, 2022. See the published version at https://doi.org/10.1038/s42005-022-00939-7.

Draft version May 19, 2021
Typeset using LaTeX **twocolumn** style in AASTeX63

The contribution of Galactic TeV pulsar wind nebulae to Fermi-LAT diffuse emission

V. Vecchiotti,[1,2] G. Pagliaroli,[1,2] and F.L. Villante[3,2]

[1] *Gran Sasso Science Institute, 67100 L'Aquila, Italy*
[2] *INFN, Laboratori Nazionali del Gran Sasso, 67100 Assergi (AQ), Italy*
[3] *University of L'Aquila, Physics and Chemistry Department, 67100 L'Aquila, Italy*

Abstract

The large-scale diffuse $\gamma-$ray flux observed by Fermi-LAT in the 1-100 GeV energy range, parameterized as $\propto E^{-\Gamma}$, has a spectral index Γ that depends on the distance from the Galactic center. This feature, if attributed to the diffuse emission produced by cosmic rays (CR) interactions with the interstellar gas, can be interpreted as the evidence of a progressive CR spectral hardening towards the Galactic center. This interpretation challenges the standard cosmic rays diffusion paradigm. We report on the implications of TeV Pulsar Wind Nebulae observed by the HESS Galactic Plane Survey in the 1-100 TeV energy range for the interpretation of Fermi-LAT data. We argue that a relevant fraction of this population cannot be resolved by Fermi-LAT in the GeV domain providing a relevant contribution to the large-scale diffuse emission, viz. the 30% of the total diffuse γ-ray emission in the inner Galaxy. This additional component naturally accounts for a large part of the spectral index variation observed by Fermi-LAT, weakening the evidence of CR spectral hardening in the inner Galaxy.

Keywords: Pulsar Wind Nebulae, Galactic Cosmic Ray

1. INTRODUCTION

Cosmic Rays (CRs) with energy below ~ 1 PeV are believed to originate in the Milky Way and to spread in the entire Galaxy due to diffusion in local magnetic fields (Gabici et al. 2019). The diffuse γ-ray emission, produced by interaction of CRs with the gas contained in the galactic disk, carries information on the energy distribution of CRs in different regions of the Galaxy.

Recent observations at GeV energies performed by Fermi-LAT suggest that the diffuse gamma-ray emission, parameterized as $\propto E^{-\Gamma}$, has a spectral index Γ in the inner Galaxy which is smaller by an amount ~ -0.2 than the value observed at the Sun position (Pothast et al. (2018), Yang et al. (2016), Acero et al. (2016)). This feature can be considered as the indirect evidence of a progressive CR spectral hardening towards the Galactic center. This conclusion, however, challenges the standard CR diffusion paradigm, in which uniform diffusion throughout the Galaxy is assumed, and would require non-standard or anomalous CR transport mechanisms, see e.g. (Recchia et al. 2016; Cerri et al. 2017). It is thus extremely important to consider any possible alternative explanations of Fermi-LAT results Nava et al. (2017).

An essential step for the observational identification of CR diffuse emission, is the evaluation of the cumulative flux produced by sources which are too faint to be resolved by Fermi-LAT. These sources are not individually detected but give rise to a large scale diffuse flux superimposed to that produced by CR interactions. To investigate the role of this additional component Acero et al. (2016) and Pothast et al. (2018) performed a source population study concluding that the diffuse flux associated to unresolved sources is not large enough to explain the spectral anomaly being below 3% at 1 GeV (20% at $\simeq 100$ GeV) of the total observed diffuse emission. Both studies are tuned on the 3FGL catalogue. As a consequence, they reproduce the population of Galactic sources observed in the GeV energy domain which is largely dominated by Pulsars. These objects have $\gamma-$ray spectra with exponential cutoff at few GeV and are expected to provide a negligible contribution to observed emission at $E \geq 10$ GeV.

In the last decade, Imaging Atmospheric Cherenkov Telescopes (IACT), like H.E.S.S. (Aharonian et al. 2006), MAGIC (Aleksić et al. 2016) and VERITAS (Weekes et al. 2002), and air shower arrays, such as

Corresponding author: Vittoria Vecchiotti
vittoria.vecchiotti@gssi.it

Argo-YBJ (Bartoli et al. 2013), Milagro (Atkins et al. 2004) and HAWC (Abeysekara et al. 2016, 2017, 2020), provided a detailed description of Galactic $\gamma-$ray emission in the energy range $0.1 - 100\,\mathrm{TeV}$. The emerging picture is that TeV Galactic sky is dominated by a population of bright sources powered by pulsar activity, such as pulsar wind nebulae (PWNe) (Abdalla et al. 2018a) or TeV halos (Linden & Buckman 2018; Sudoh et al. 2019; Giacinti et al. 2020), whose properties can be effectively constrained by observations at TeV energies, see e.g. (Cataldo et al. 2020; Steppa & Egberts 2020). These objects are clearly expected to emit also in the GeV energy domain where, however, population studies are more difficult because different kinds of sources dominate the observed emission.

In this paper, we took advantage of the constraints provided by HESS Galactic Plane Survey (HGPS) to discuss the implications of TeV PWNe for the interpretation of Fermi-LAT data in the GeV domain. We quantify the contribution of unresolved TeV PWNe to large scale diffuse emission observed by Fermi-LAT at different distances from the Galactic center. We show that the inclusion of this additional component can strongly affect the reconstructed CR energy distribution from Fermi-LAT data, weakening the evidence of a progressive hardening of the cosmic-ray spectrum toward the Galactic center.

2. RESULTS

Pulsar wind nebulae are expected to contribute to γ observations both in the GeV and TeV energy domains. We indicate with Φ_{GeV} (Φ_{TeV}) the integrated source flux in the energy range $1-100\,\mathrm{GeV}$ ($1-100\,\mathrm{TeV}$) probed by Fermi-LAT (H.E.S.S.). We assume that all the sources in the considered population have approximately the same emission spectrum, described by a broken power-law with different spectral indexes β_{GeV} and β_{TeV} in the GeV and TeV energy domain and with a transition energy $E_0 = 0.3\,\mathrm{TeV}$ located between the ranges probed by Fermi-LAT and H.E.S.S. This spectral shape leads to a consistent description of HGPS and 3FGL catalogue for $\beta_{\mathrm{GeV}} \leq 2$, see Method for a detailed discussion. In this assumption, the ratio

$$R_\Phi \equiv \frac{\Phi_{\mathrm{GeV}}}{\Phi_{\mathrm{TeV}}} \tag{1}$$

between fluxes emitted by a given source in different energy domains is fixed and can be calculated as a function of β_{GeV} and β_{TeV} as it is discussed in Section 4.

At high energies ($E \geq E_0$), we take the average spectrum observed by HESS (Abdalla et al. 2018b) as a reference, i.e. we assume that all sources have $\beta_{\mathrm{TeV}} = 2.3$. The index β_{GeV} is instead determined by requiring realistic values for the flux ratio R_Φ. In our calculations, we take as a reference the values $R_\Phi = 500$ and 1000 that correspond to $\beta_{\mathrm{GeV}} = 1.7$ and 1.9, respectively. The adopted values for R_Φ are validated by considering the average observational properties of PWNe observed by Fermi-LAT and H.E.S.S. in the GeV/TeV domain, see Section 4 for details. Moreover, the corresponding spectral shapes are consistent with theoretical predictions of γ-ray emission from PWNe, as e.g. discussed by Bucciantini et al. (2011); Torres et al. (2014).

The properties of the considered source population can be constrained by observation in the TeV energy domain. Following Cataldo et al. (2020), PWNe distribution is described by:

$$\frac{dN}{d^3r\, dL_{\mathrm{TeV}}} = \rho\left(\mathbf{r}\right) Y_{\mathrm{TeV}}\left(L_{\mathrm{TeV}}\right) \tag{2}$$

where r indicates the source distance from the Galactic Center. The function $\rho(\mathbf{r})$ describes the spatial distribution of the sources and it is conventionally normalized to one when integrated in the entire Galaxy. It is assumed to be proportional to the pulsar distribution in the Galactic plane parameterized by Lorimer et al. (2006). The source density along the direction perpendicular to the Galactic plane is assumed to scale as $\exp\left(-\left|z\right|/H\right)$ where $H = 0.2$ kpc represents the thickness of the Galactic disk.

The function $Y_{\mathrm{TeV}}(L_{\mathrm{TeV}})$ gives the source intrinsic luminosity distribution in the TeV energy domain. It is parameterized as a power-law:

$$Y_{\mathrm{TeV}}(L_{\mathrm{TeV}}) = \frac{R\,\tau\,(\alpha-1)}{L_{\mathrm{TeV,\,Max}}} \left(\frac{L_{\mathrm{TeV}}}{L_{\mathrm{TeV,\,Max}}}\right)^{-\alpha} \tag{3}$$

that extends in the luminosity range $L_{\mathrm{TeV,\,Min}} \leq L_{\mathrm{TeV}} \leq L_{\mathrm{TeV,\,Max}}$, see e.g. Strong (2007). This distribution is naturally obtained for a population of *fading* sources, such as PWNe or TeV Halos, produced with a constant rate R and having intrinsic luminosity that decreases over a time scale τ, see Methods for details. As working hypotheses, two different values for the luminosity index, $\alpha = 1.5$ and $\alpha = 1.8$, are considered. By fitting the flux, latitude and longitude distribution of bright sources in the HGPS catalogue (and assuming that the PWNe birth rate is equal to that of core-collapse SN explosions, i.e. $R = 0.019\ \mathrm{yr}^{-1}$), one obtains $L_{\mathrm{TeV,\,Max}} = 4.9 \cdot 10^{35}\,\mathrm{erg\,cm^{-2}\,s^{-1}}$ ($L_{\mathrm{TeV,\,Max}} = 6.8{\cdot}10^{35}\,\mathrm{erg\,cm^{-2}\,s^{-1}}$) and $\tau = 1.8{\cdot}10^3$ y ($\tau = 0.5{\cdot}10^3$ y) for $\alpha = 1.5$ ($\alpha = 1.8$) (Cataldo et al. 2020).

The determination of $L_{\mathrm{TeV,\,Max}}$ and τ by HGPS data allows us to constrain the properties of PWNe population in the TeV domain. As an example, the total flux

Table 1. *The cumulative flux of resolved (Φ^{R}_{GeV}) and unresolved (Φ^{NR}_{GeV}) TeV PWNe in the GeV domain for $\alpha = 1.8$ and for the two different values of R_Φ considered in our analysis. The Fermi-LAT diffuse emission Φ^{diff}_{GeV} is shown in the first column (Pothast et al. 2018). The numbers in brackets give the ratios $\Phi^{NR}_{GeV}/\Phi^{diff}_{GeV}$ in different galactocentric rings.*

	Φ^{diff}_{GeV} $(cm^{-2}\ s^{-1})$	Φ^{NR}_{GeV} $(cm^{-2}\ s^{-1})$		Φ^{R}_{GeV} $(cm^{-2}\ s^{-1})$	
		$R_\Phi = 500$	$R_\Phi = 1000$	$R_\Phi = 500$	$R_\Phi = 1000$
$1.7 - 4.5$ kpc	3.86×10^{-7}	6.63×10^{-8} (17%)	1.15×10^{-7} (29.9%)	2.78×10^{-8}	7.29×10^{-8}
$4.5 - 5.5$ kpc	3.11×10^{-7}	3.8×10^{-8} (12.2%)	6.62×10^{-8} (21.2%)	2.1×10^{-8}	5.2×10^{-8}
$5.5 - 6.5$ kpc	5.09×10^{-7}	4.24×10^{-8} (8.3%)	7.37×10^{-8} (14.4%)	3.0×10^{-8}	7.14×10^{-8}
$6.5 - 7.0$ kpc	2.57×10^{-7}	2.28×10^{-8} (8.8%)	3.96×10^{-8} (15.3%)	2.08×10^{-8}	4.77×10^{-8}
$7.0 - 8.0$ kpc	7.7×10^{-7}	5.29×10^{-8} (6.8%)	9.21×10^{-8} (11.9%)	7.03×10^{-8}	1.54×10^{-7}
$8.0 - 10.0$ kpc	3.84×10^{-6}	9.69×10^{-8} (2.5%)	1.68×10^{-7} (4.3%)	2.24×10^{-7}	4.74×10^{-7}
$10.0 - 16.5$ kpc	7.68×10^{-7}	3.0×10^{-8} (3.9%)	5.24×10^{-8} (6.8%)	1.9×10^{-8}	4.56×10^{-8}
$16.5 - 50.0$ kpc	4.44×10^{-8}	7.73×10^{-10} (1.7%)	1.38×10^{-9} (3.1%)	9.23×10^{-11}	3.44×10^{-10}
$0.0 - 50.0$ kpc	6.89×10^{-6}	3.55×10^{-7}(5.1%)	6.18×10^{-7} (8.9%)	4.15×10^{-7}	9.23×10^{-7}

Φ^{tot}_{TeV} produced at Earth by the considered sources can be calculated as a function of $L_{TeV,\,Max}$ and τ by using eq. (12), as discussed in Section 4. The total flux produced at Earth by TeV PWNe in the GeV domain depends also on the parameter R_Φ and it is given by:

$$\Phi^{tot}_{GeV} = R_\Phi\, \Phi^{tot}_{TeV}. \qquad (4)$$

A fraction of this flux is emitted by sources which are too faint to be individually resolved by Fermi-LAT and contribute to the large scale diffuse emission observed by this experiment. The unresolved contribution can be calculated as:

$$\Phi^{NR}_{GeV} = \int_0^{\Phi^{th}_{GeV}} d\Phi_{GeV}\ \Phi_{GeV}\ \frac{dN}{d\Phi_{GeV}} \qquad (5)$$

where $dN/d\Phi_{GeV}$ is the source flux distribution in the GeV domain while $\Phi^{th}_{GeV} = 10^{-9}\,cm^{-2}\,s^{-1}$ is the Fermi-LAT detection threshold (Acero et al. 2015).

In the last line of Tab.1, we give the cumulative flux Φ^{NR}_{GeV} ($\Phi^{R}_{GeV} = \Phi^{tot}_{GeV} - \Phi^{NR}_{GeV}$) produced by TeV PWNe that are not resolved (resolved) by Fermi-LAT for the two assumed values $R_\Phi = 500$ and 1000. These fluxes are compared with the total large scale diffuse emission Φ^{diff}_{GeV} detected by Fermi-LAT (see second column in Tab.1) in the $1 - 100$ GeV energy range and determined by Pothast et al. (2018) by using 9.3 years of Fermi-LAT Pass 8 data[1]. We see that unresolved emission by PWNe corresponds to a fraction $\sim 5\%$ (for $R_\Phi = 500$) and $\sim 9\%$ (for $R_\Phi = 1000$) of the total large scale diffuse emission. The above predictions are obtained by assuming that the source luminosity distribution index is $\alpha = 1.8$ to conform with previous analyses on the subject (Acero et al. 2016; Pothast et al. 2018) that have been performed under this hypothesis. Results for $\alpha = 1.5$ are reported as additional material in the last section.

In order to probe the radial dependence of the PWNe contribution, we repeat our calculations by considering the Galactocentric rings adopted by Pothast et al. (2018). The flux produced by unresolved TeV PWNe in each ring is compared with the Fermi-LAT diffuse emission from the same region. As we see from Tab. 1, the unresolved contribution becomes more relevant in the central rings, due the fact that the source density (and the average distance from the Sun position) is larger. In the most internal region ($1.7 \leq r \leq 4.5$kpc), unresolved sources account for about $\sim 20\%$ ($\sim 30\%$) of the Fermi-LAT diffuse emission for $R_\Phi = 500$ ($R_\Phi = 1000$)[2]. This clearly shows that this component is not negligible and cannot be ignored in the interpretation of Fermi-LAT diffuse emission data.

The effect of the unresolved TeV PWNe population on the determination of CR diffuse emission is discussed in Fig. 1. Black data points show the total diffuse $\gamma-$ray flux observed by Fermi-LAT in each galactocentric ring given by Pothast et al. (2018) in 25 log-spaced energy

[1] The energy integrated fluxes have been obtained by interpolating the points presented in Pothast et al. (2018) and integrating in the energy range $1 - 100$ GeV.

[2] We do not consider the central region $r \leq 1.7$ because it is affected by large systematic errors, as it is discussed in Pothast et al. (2018).

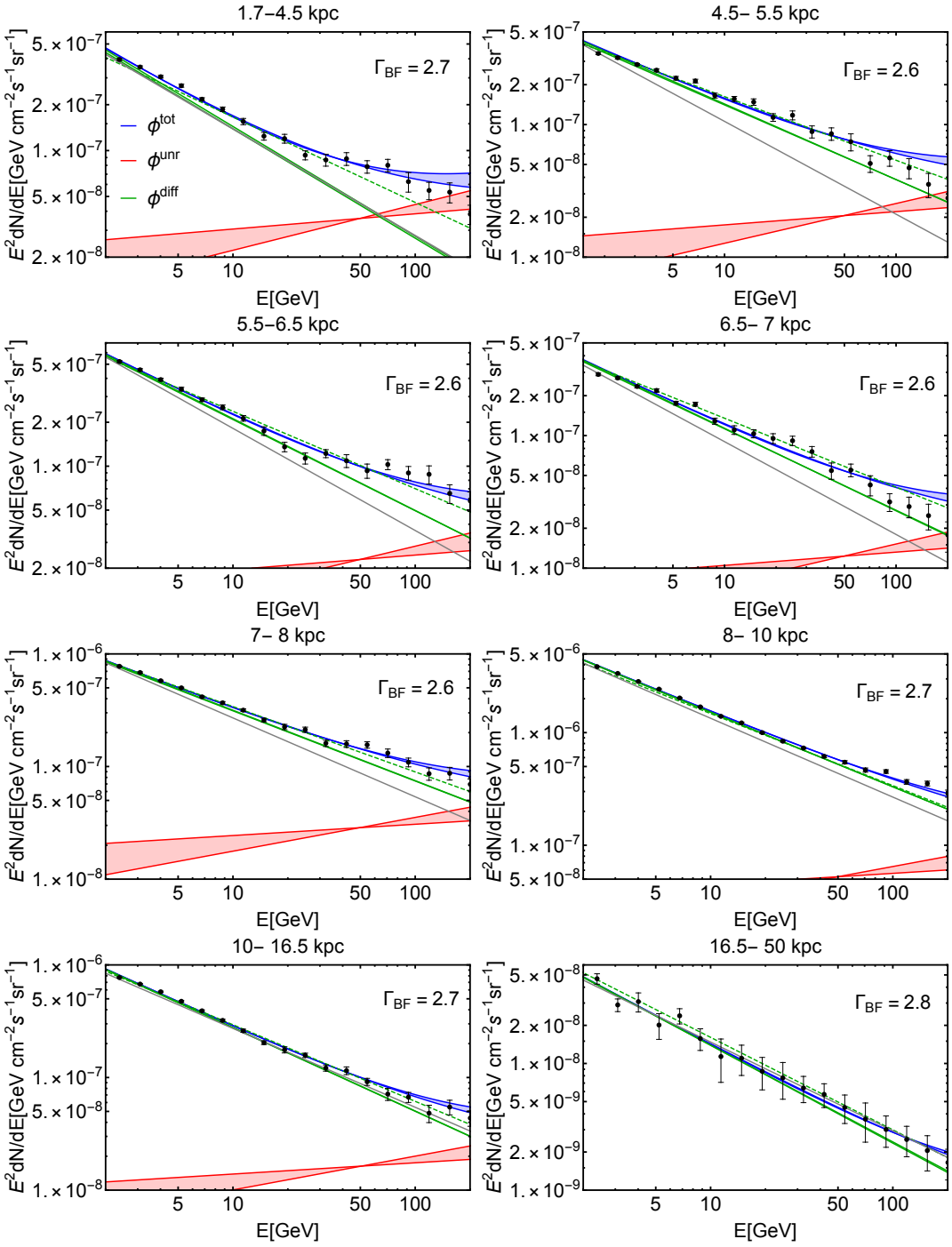

Figure 1. *Black data points show the total diffuse γ-ray emission measured by Fermi-LAT in each galactocentric ring Pothast et al. (2018). The red lines represent the predicted contribution of unresolved TeV PWNe for $\alpha = 1.8$. Green lines show the diffuse CR emission inferred by fitting the data with (solid) and without (dashed) including the PWNe contribution. Blue lines represent the total gamma fluxes predicted as a function of the energy for $\alpha = 1.8$. The gray lines show a power-law with an index of 2.7 for comparison.*

bins between $0.34 - 228.65$ GeV and in the latitude window $|b| < 20.25°$. These data have been fitted with a single power-law $\propto E^{-\Gamma_1}$ by Pothast et al. (2018), obtaining the green dashed lines reported in Fig.1. The decrease of the best-fit spectral indexes Γ_1 in the inner rings with respect to the locally observed value, see Tab.2, has been considered as the evidence of a progressive large-scale hardening of CRs spectrum toward the

Galactic Center. The same conclusion was obtained by previous analyses on the subject (Acero et al. 2016; Yang et al. 2016) performed by using a similar approach. One can get a visual perception of the situation by comparing the green dashed lines with the grey solid lines in Fig.1 that describe power laws with spectral index fixed at the local value, i.e. ~ 2.7, suitably normalized to reproduce the observed flux at 2 GeV.

The above conclusion is only valid if unresolved source contribution is negligible, so that the total observed emission can be identified with the "truly" diffuse component produced by CR interaction with interstellar matter. This assumption is, however, not adequate in the inner Galaxy, as it is shown by the red solid lines in Fig.1 that give the unresolved PWNe contribution as function of energy for $R_\Phi = 500$ and 1000. The parameter R_Φ is linked to the source spectral index $\beta_{\rm GeV}$, so that different values for it also imply a different slope of PWNe contribution, being $\beta_{\rm GeV} = 1.7$ and 1.9 for $R_\Phi = 500$ and 1000, respectively. The red shaded area can be considered as the theoretical uncertainty associated to the assumed sources spectrum.

We improve with respect to previous analyses (Pothast et al. 2018; Acero et al. 2016; Yang et al. 2016) by fitting the Fermi-LAT data with the additional contribution due to unresolved PWNe. The truly diffuse gamma-ray flux due to CR interactions is still parameterized as a single power-law (the number of degrees of freedom in the fit is not changed) but the total flux, described with blue lines in Fig.1, is obtained as the sum of CR diffuse emission plus the unresolved PWNe contribution. The best-fits spectral indexes Γ_{BF} for CR diffuse emission in each ring are reported in Tab.2 for $R_\Phi = 500$ and 1000. These correspond to the thick solid green lines reported in Fig.1. The obtained values for Γ_{BF} are mildly dependent on the assumed R_Φ.

In each panel of Fig.1, we report the average value of $\Gamma_{\rm BF}$ in the two cases $R_\Phi = 500$ and 1000, in order that the reader can quickly compare the results obtained at different distances from the Galactic center. It is evident that the unresolved PWNe contribution affects the reconstructed properties of CR diffuse emission, weakening considerably the evidence of CR spectral hardening in the central region of the Galaxy. In order to quantify this point, we show in Fig.2, the difference between the spectral index of the truly diffuse component obtained by fitting the data with and without unresolved emission. In other words, we show the quantity $\Delta\Gamma = \Gamma_{BF} - \Gamma_1$ where Γ_1 is the best-fit for the truly diffuse emission obtained by Pothast et al. (2018) while Γ_{BF} is the best-fit for the same quantity obtained in this work. The reported error bar takes also into account the effect of possible variations of the parameter R_Φ within the range $R_\Phi = 500 - 1000$. The inclusion of unresolved PWNe strongly affects the spectral index of CR diffuse emission that can be increased up to $\Delta\Gamma = 0.17$ in the central ring adjusting it to the locally observed value, i.e. ~ 2.7. In the other rings the cosmic ray spectrum still show a residual difference with the local value. The evidence of spectral hardening toward the Galactic Center is however less pronounced.

Table 2. *Spectral indexes of the CR diffuse emission obtained by fitting the Fermi-LAT data with (Γ_{BF}) and without (Γ_1) TeV PWNe unresolved contribution. The indexes Γ_1 coincide with those obtained by Pothast et al. (2018).*

Ring	Γ_1	Γ_{BF}	$\alpha = 1.8$
		$R_\Phi = 500$	$R_\Phi = 1000$
$1.7 - 4.5$ kpc	2.56 ± 0.02	2.72 ± 0.01	2.72 ± 0.01
$4.5 - 5.5$ kpc	2.48 ± 0.02	2.57 ± 0.01	2.56 ± 0.01
$5.5 - 6.5$ kpc	2.54 ± 0.04	2.63 ± 0.01	2.63 ± 0.01
$6.5 - 7$ kpc	2.54 ± 0.01	2.62 ± 0.01	2.61 ± 0.02
$7 - 8$ kpc	2.57 ± 0.01	2.625 ± 0.008	2.623 ± 0.008
$8 - 10$ kpc	2.642 ± 0.003	2.663 ± 0.003	2.662 ± 0.004
$10 - 16.5$ kpc	2.696 ± 0.008	2.743 ± 0.008	2.740 ± 0.009
$16.5 - 50$ kpc	2.72 ± 0.03	2.77 ± 0.04	2.76 ± 0.03

3. CONCLUSIONS

The TeV Galactic sky is dominated by a population of bright young PWNe whose properties are constrained by present HESS Galactic Plane Survey (HGPS) data. We predict the cumulative emission produced by this population in the GeV domain within a phenomenological model that is based on the average spectral properties of PWNe. We argue that a relevant fraction of the TeV PWNe population cannot be resolved by Fermi-LAT. The γ-ray flux due to unresolved TeV PWNe and the truly diffuse emission, due to CR interactions with the interstellar gas, add up contributing to shape the radial and spectral behaviour of the total diffuse γ-ray emission observed by Fermi-LAT.

The spatial distribution of TeV PWNe, peaking around $r = 4$ kpc from the Galactic Center, combined with the detector flux threshold modulate the relative contribution of unresolved sources in different Galactocentric rings. In particular the relevance of this component increases in the inner rings where the total diffuse emission has a different spectral distribution with respect to the local one. Previous analyses neglected the contribution due to unresolved PWNe and interpreted the observed spectral behaviour of the total diffuse emission as an indirect evidence for CR spectral hardening

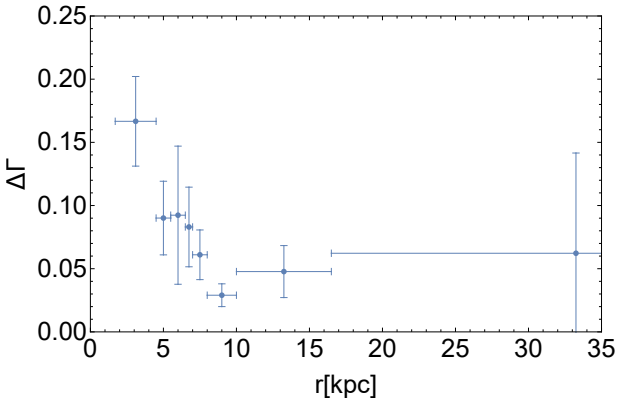

Figure 2. *The difference* $\Delta\Gamma$ *between the spectral index of the truly diffuse emission obtained in different Galactocentric rings by fitting the Fermi-LAT data with/without the contribution of unresolved PWNe.*

toward the Galactic center (Acero et al. 2016; Yang et al. 2016; Pothast et al. 2018). We have shown that the emergence of PWNe unresolved component in the central region, which is characterized by an average spectral index $\beta_{\rm GeV} < 2.$, can strongly affect this conclusion, by naturally accounting for (a large part of) the spectral index observed variation as a function of r. Our results could also solve the tension discussed in Cataldo et al. (2019), between total γ-ray emission measured by HESS, Milagro, Argo and HAWC and that obtained by implementing CR spectral hardening. Moreover, they are in agreement with very recent results obtained by (Peron et al. 2021) following a completely different approach based on giant molecular clouds.

4. METHOD

Flux and luminosity ratios—The sources considered in this work are expected to contribute to observations both in the GeV and TeV energy domains. We indicate with $\Phi_{\rm GeV}$ ($\Phi_{\rm TeV}$) and $L_{\rm GeV}$ ($L_{\rm TeV}$) the integrated source flux and luminosity in the energy range $1-100\,{\rm GeV}$ ($1-100\,{\rm TeV}$) probed by Fermi-LAT (H.E.S.S.). We assume for simplicity that all the sources in the considered population have approximately the same emission spectrum. This automatically implies that the ratio $R_\Phi \equiv \Phi_{\rm GeV}/\Phi_{\rm TeV}$ between fluxes emitted in different energy domains by a given source is fixed. The relationship between intrinsic luminosity and flux produced at Earth is generically written as:

$$\Phi_{\rm X} = \frac{L_{\rm X}}{4\pi r^2 E_{\rm X}} \qquad (6)$$

where r is the source distance, $E_{\rm X}$ is the average energy of emitted photons and ${\rm X} = {\rm GeV}, {\rm TeV}$ indicates the considered energy range.

Source spectrum—The source emission spectrum $\varphi(E)$ can have a different behaviour at GeV and TeV energies. We take this into account by parameterizing it with a broken power-law with different spectral indexes $\beta_{\rm GeV}$ and $\beta_{\rm TeV}$ in the GeV and TeV energy domain and with a transition at the energy $E_0 = 0.3\,{\rm TeV}$ located between the ranges probed by Fermi-LAT and HGPS. Even if our approach is completely phenomenological, the postulated spectral behaviour is expected from a theoretical point of view. We are indeed considering the hypothesis, suggested e.g. by Sudoh et al. (2019), that most of the bright TeV sources are young PWNe and/or TeV halos. In this scenario, the observed gamma-ray emission is produced by IC scattering of HE electron and positrons on background photons (CMB, starlight, infrared). In the Thompson regime, this naturally produces hard gamma-ray emission with spectral index $\beta \sim (p+1)/2$ where p is the electron/positron spectral index. At TeV energy, it produces instead a softer gamma-ray spectrum either due to the Klein-Nishina regime $\beta \sim (p+1)$ or to electron/positron energy losses, see e.g.(Bucciantini et al. 2011; Torres et al. 2014; Sudoh et al. 2021).

In the assumption of a broken power-law for the gamma ray spectrum, the flux ratio R_Φ can be expressed as a function of $\beta_{\rm GeV}$ and $\beta_{\rm TeV}$, obtaining:

$$R_\Phi = \frac{1-\beta_{\rm TeV}}{1-\beta_{\rm GeV}} \frac{\left[(\epsilon^{\rm sup}_{\rm GeV})^{1-\beta_{\rm GeV}} - (\epsilon^{\rm inf}_{\rm GeV})^{1-\beta_{\rm GeV}}\right]}{\left[(\epsilon^{\rm sup}_{\rm TeV})^{1-\beta_{\rm TeV}} - (\epsilon^{\rm inf}_{\rm TeV})^{1-\beta_{\rm TeV}}\right]} \qquad (7)$$

where $\epsilon^{\rm inf}_{\rm GeV} \equiv (1.0\,{\rm GeV}/E_0)$ and $\epsilon^{\rm sup}_{\rm GeV} \equiv (100\,{\rm GeV}/E_0)$ ($\epsilon^{\rm inf}_{\rm TeV} \equiv (1.0\,{\rm TeV}/E_0)$ and $\epsilon^{\rm sup}_{\rm TeV} \equiv (100\,{\rm TeV}/E_0)$) are the lower and upper bounds of the GeV (TeV) energy domains. Realistic values for this parameter can be obtained from observations by considering the ensemble of PWNe that are firmly identified both in the 3FGL and HGPS catalogues (6 objects). By taking the ratio of the integrated fluxes $\Phi_{\rm GeV}$ measured by Fermi-LAT with the values $\Phi_{\rm TeV}$ reported by H.E.S.S., we obtain $R_\Phi \leq 1200$ (with an average value $R_\Phi \simeq 700$). In our calculations, we take as a reference the values $R_\Phi = 500$ and 1000 that correspond to $\beta_{\rm GeV} \simeq 1.7$ ($\beta_{\rm GeV} \simeq 1.9$), see Eq.(7).

Luminosity distribution—In the following, we focus on the TeV-luminosity function since this can be effectively constrained by HGPS observational results (Cataldo et al. 2020). The function $Y_{\rm TeV}(L_{\rm TeV})$ is parameterized as descibred in Eq 3. This distribution is naturally obtained for a population of *fading* sources with intrinsic luminosity that decreases over a time scale τ according to:

$$L_{\rm TeV}(t) = L_{\rm TeV,\,Max}\left(1+\frac{t}{\tau}\right)^{-\gamma} \qquad (8)$$

where t indicates the time passed since source formation. In this assumption, the exponent of the luminosity distribution is given by $\alpha = 1/\gamma + 1$.

The above description can be applied to potential TeV sources in the Galaxy, such as PWNe (Gaensler & Slane 2006) or TeV Halos (Linden & Buckman 2018), which are connected with the explosion of core-collapse SN and the formation of a pulsar. The birth rate of these objects is similar to that of SN explosions in our Galaxy, i.e. $R \simeq R_{\rm SN} = 0.019\,{\rm yr}^{-1}$ as recently measured by Diehl et al. (2006). If gamma-ray emission is powered by pulsar activity, the TeV-luminosity can be connected to the pulsar spin-down power, i.e.:

$$L_{\rm TeV} = \lambda\,\dot{E} \tag{9}$$

where $\lambda \leq 1$ and:

$$\dot{E} = \dot{E}_0 \left(1 + \frac{t}{\tau_{\rm sd}}\right)^{-2} \tag{10}$$

for energy loss dominated by magnetic dipole radiation (braking index $n = 3$). This implies that the fading timescale is determined by the pulsar spin-down time scale, i.e. $\tau = \tau_{\rm sd}$. Moreover, if the efficiency of TeV emission does not depend on time ($\lambda \sim$ const), the exponent in Eq. (8) is $\gamma = 2$, that corresponds to a source luminosity function $Y_{\rm TeV}(L_{\rm TeV}) \propto L_{\rm TeV}^{-1.5}$. The possibility of λ being correlated to the spin-down power, i.e. $\lambda = \lambda_0(\dot{E}/\dot{E}_0)^{\delta}$, was suggested by Abdalla et al. (2018a) that found $L_{\rm TeV} = \lambda\,\dot{E} \propto \dot{E}^{1+\delta}$ with $1+\delta = 0.59 \pm 0.21$ by studying a sample of PWNe in the HPGS catalogue. In this case, one obtains $\gamma \simeq 1.2$ in Eq. (8) that corresponds to a source luminosity function $Y_{\rm TeV}(L_{\rm TeV}) \propto L_{\rm TeV}^{-1.8}$. These two scenarios ($\alpha = 1.5$ and $\alpha = 1.8$) are considered as working hypotheses in this paper.

Consistency among HGPS and Fermi-LAT catalogues— The implications of the TeV PWN population at GeV energies depend on the parameter R_Φ which is related to the assumed source spectrum. The reference values $R_\Phi = 500$ and $R_\Phi = 1000$ (corresponding to $\beta_{\rm GeV} = 1.7$ and 1.9, respectively) can be further validated by comparing the predicted source flux distribution in the GeV domain with the results of the Fermi-LAT 3FGL catalogue. The two shaded bands in Fig.3 show the cumulative number $N(\Phi_{\rm GeV})$ of expected sources in the latitude range $|b| \leq 20.25^\circ$ with flux larger than $\Phi_{\rm GeV}$ for two different values of the power-law index of the luminosity function ($\alpha = 1.5$ and 1.8). Namely, the red (blue) shaded band is obtained by assuming the best-fit values $L_{\rm TeV,\,Max} = 4.9 \cdot 10^{35}\,{\rm erg\,cm^{-2}\,s^{-1}}$ ($L_{\rm TeV,\,Max} = 6.8 \cdot 10^{35}\,{\rm erg\,cm^{-2}\,s^{-1}}$) and $\tau = 1.8 \cdot 10^3$ y ($\tau = 0.5 \cdot 10^3$ y) for $\alpha = 1.5$ ($\alpha = 1.8$) given in Cataldo et al. (2020) and by varying the flux ratio in the range $500 \leq R_\Phi \leq 1000$. Theoretical predictions can be compared with observational results. It should be remarked that, while PWNe provide the prominent contribution of the observed emission at TeV energies, they are instead a subdominant component in the GeV domain. The 3FGL catalogue includes 3033 sources which are mostly extragalactic objects (Acero et al. 2015). The total number of identified and/or associated Galactic sources is 266. The largest source class, including 167 objects, is given by pulsars that tipically have soft emission spectra with cut-off at few GeV and are not expected to contribute to the population of TeV emitting sources potentially detectable by HGPS. In addition to pulsars, the 3FGL catalogue encompasses 11 PWNe, 23 SNRs, and 49 objects (labelled as SPP) of unknown nature but overlapping with known SNRs or PWNe. The magenta in Fig.3 corresponds to the distribution of PWNe included in 3FGL while the black line also include SPP sources. The SPP source class is not expected to fully correspond to the population considered in this work; it can be however regarded as an upper limit for theoretical predictions. We see that a reasonable agreement exists with theoretical expectations, supporting the phenomenological description adopted in this paper. As additional check, we have verified that theoretical predictions are consistent with the more recent 4FGL catalogue Abdollahi et al. (2020). We also note that the performed comparison provides by itself a proof that the average spectral index $\beta_{\rm GeV}$ of PWNe at GeV energies should be smaller than the value $\beta_{\rm TeV} = 2.3$ observed in the TeV domain. Indeed, if we assume that source spectrum is described by undistorted power-law with spectral index $\beta_{\rm TeV} \sim 2.3$, we obtain $R_\Phi = 10^{3\,(\beta_{\rm TeV}-1)} \sim 10^4$. Considering that bright sources in the HGPS catalogue have fluxes $\Phi_{\rm TeV} \sim 10^{-11}\,{\rm cm^{-2}\,s^{-1}}$, we should expect an ensemble of sources with fluxes $\Phi_{\rm GeV} \sim 10^{-7}\,{\rm cm^{-2}\,s^{-1}}$ in the GeV domain. This is not observed by Fermi-LAT, indicating that TeV galactic sources typically have a spectral break and harder emission spectrum below ~ 1 TeV. Coherently with this conclusion, most of the PWNe in the 3FGL catalogue have a spectral indexes ≤ 2 at GeV energies.

Total luminosity and flux—The total luminosity produced by the considered population in the TeV domain is given as a function of $L_{\rm TeV,\,Max}$ and τ by:

$$L_{\rm TeV}^{\rm MW} = \frac{\mathcal{N}\,L_{\rm TeV,\,Max}}{(2-\alpha)}\left[1 - \Delta^{\alpha-2}\right] \tag{11}$$

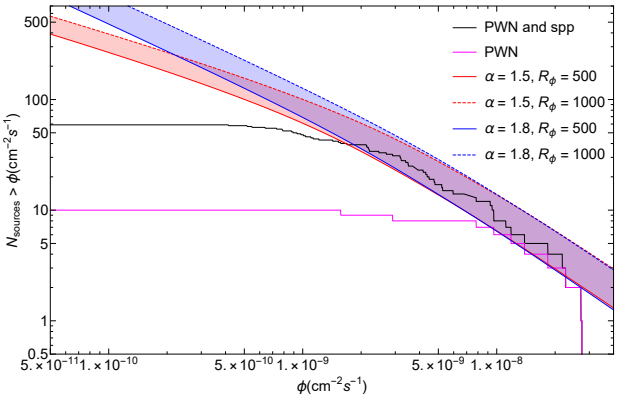

Figure 3. *The cumulative number $N(\Phi_{\rm GeV})$ of sources with fluxes larger than $\Phi_{\rm GeV}$ predicted in our model and in the latitude range $|b| \leq 20.25°$. The red (blue) band is obtained by assuming $\alpha = 1.5$ ($\alpha = 1.8$) and by considering $500 \leq R_\Phi \leq 1000$. The magenta line represents the cumulative number of PWNe with fluxes larger than $\Phi_{\rm GeV}$ in the 3FGL catalogue. The black line also includes SPP sources.*

where $\mathcal{N} = R\,\tau\,(\alpha - 1)$ and $\Delta \equiv L_{\rm TeV,\,Max}/L_{\rm TeV,\,Min}$[3]. The flux in the TeV domain produced at Earth by all sources included in a fixed observational window (OW) can be expressed as:

$$\Phi^{\rm tot}_{\rm TeV} = \xi\,\frac{L^{\rm MW}_{\rm TeV}}{4\pi E_{\rm TeV}}\,\langle r^{-2}\rangle \tag{12}$$

where the parameter ξ, which is defined as

$$\xi \equiv \int_{\rm OW} d^3r\,\rho(\mathbf{r}), \tag{13}$$

represents the fraction of sources of the considered population which are included in the OW, while the quantity

$$\langle r^{-2}\rangle \equiv \frac{1}{\xi}\int_{\rm OW} d^3r\,\rho(\mathbf{r})\,r^{-2} \tag{14}$$

is the average value of their inverse square distance.

The total flux produced by the considered population in the GeV domain can be calculated as a function of the parameter R_Φ (for fixed values of $L_{\rm TeV,\,Max}$ and τ) and it is given by

$$\Phi^{\rm tot}_{\rm GeV} = R_\Phi\,\Phi^{\rm tot}_{\rm TeV} \tag{15}$$

Unresolved source contribution—Faint sources that produce a flux at Earth below the Fermi-LAT observation threshold $\Phi^{\rm th}_{\rm GeV}$ are not resolved and contribute to the large scale diffuse emission from the Galaxy. This contribution can be evaluated as:

$$\Phi^{\rm NR}_{\rm GeV} = \int_0^{\Phi^{\rm th}_{\rm GeV}} d\Phi_{\rm GeV}\,\Phi_{\rm GeV}\,\frac{dN}{d\Phi_{\rm GeV}} \tag{16}$$

where $dN/d\Phi_{\rm GeV}$ is the source flux distribution expected in GeV domain. This is connected to the source flux distribution in TeV domain by the R_Φ parameter, according to:

$$\frac{dN}{d\Phi_{\rm GeV}} = \frac{1}{R_\Phi}\,\frac{dN}{d\Phi_{\rm TeV}}\,(\Phi_{\rm GeV}/R_\Phi) \tag{17}$$

The latter can be calculated as a function of $L_{\rm TeV,\,Max}$ and τ by using:

$$\frac{dN}{d\Phi_{\rm TeV}} = \int dr\;4\pi r^4 E_{\rm TeV}\;Y_{\rm TeV}(4\pi r^2 E_{\rm TeV}\Phi_{\rm TeV})\;\overline{\rho}(r), \tag{18}$$

where $\overline{\rho}(r) \equiv \int_{\rm OW} d\Omega\;\rho(r,\mathbf{n})$. As it is discussed in Cataldo et al. (2020), the flux distribution scales as $dN/d\Phi_{\rm TeV} \propto \Phi^{-\alpha}_{\rm TeV}$ for $\Phi_{\rm TeV} \to 0$ and $dN/d\Phi_{\rm TeV} \propto \Phi^{-5/2}_{\rm TeV}$ for $\Phi_{\rm TeV} \to \infty$. This implies that $\Phi^{\rm NR}_{\rm GeV} \propto R^{\alpha-1}_\Phi$, if $L_{\rm TeV,\,Max}$ and τ are fixed, as it can be understood by using the low-flux scaling of $dN/d\Phi_{\rm TeV}$.

5. ACKNOWLEDGEMENT

We thanks Daniele Gaggero and Mart Pothast for providing us the Fermi-LAT data points of the total gamma ray diffuse emission. The work of GP and FLV is partially supported by the research grant number 2017W4HA7S "NAT-NET: Neutrino and Astroparticle Theory Network" under the program PRIN 2017 funded by the Italian Ministero dell'Istruzione, dell'Universita' e della Ricerca (MIUR).

[3] Unless otherwise specified, we quote results obtained for $\Delta \to \infty$ that can be easily recalculated by using the above equation, if other values are considered

REFERENCES

Abdalla, H., Abramowski, A., Aharonian, F., et al. 2018a, Astron. Astrophys., 612, A2, doi: 10.1051/0004-6361/201629377

—. 2018b, Astron. Astrophys., 612, A1, doi: 10.1051/0004-6361/201732098

Abdollahi, S., et al. 2020, Astrophys. J. Suppl., 247, 33, doi: 10.3847/1538-4365/ab6bcb

Abeysekara, A. U., Alfaro, R., Alvarez, C., et al. 2016, Astrophys. J., 817, 3, doi: 10.3847/0004-637X/817/1/3

Abeysekara, A. U., et al. 2017, Astrophys. J., 843, 40, doi: 10.3847/1538-4357/aa7556

Abeysekara, A. U., Albert, A., Alfaro, R., et al. 2020, Phys. Rev. Lett., 124, 021102, doi: 10.1103/PhysRevLett.124.021102

Acero, F., M. Ackermann(DESY), M., Ajello, Albert, A., et al. 2015, Astrophys. J. Suppl., 218, 23, doi: 10.1088/0067-0049/218/2/23

Acero, F., Ackermann, M., Ajello, M., et al. 2016, Astrophys. J. Suppl., 223, 26, doi: 10.3847/0067-0049/223/2/26

Aharonian, F., Akhperjanian, A. G., Bazer-Bachi, A. R., et al. 2006, Astrophys. J., 636, 777, doi: 10.1086/498013

Aleksić, J., Ansoldi, S., Antonelli, L., et al. 2016, Astropart. Phys., 72, 76, doi: 10.1016/j.astropartphys.2015.02.005

Atkins, R., Benbow, W., Berley, D., et al. 2004, Astrophys. J., 608, 680, doi: 10.1086/420880

Bartoli, B., Bernardini, P., Bi, X. J., et al. 2013, Astrophys. J., 779, 27, doi: 10.1088/0004-637X/779/1/27

Bucciantini, N., Arons, J., & Amato, E. 2011, Mon. Not. Roy. Astron. Soc., 410, 381, doi: 10.1111/j.1365-2966.2010.17449.x

Cataldo, M., Pagliaroli, G., Vecchiotti, V., & Villante, F. L. 2019, JCAP, 12, 050, doi: 10.1088/1475-7516/2019/12/050

—. 2020, Astrophys. J., 904, 85, doi: 10.3847/1538-4357/abc0ee

Cerri, S. S., Gaggero, D., Vittino, A., Evoli, C., & Grasso, D. 2017, JCAP, 10, 019, doi: 10.1088/1475-7516/2017/10/019

Diehl, R., Halloin, H., Kretschmer, K., et al. 2006, Nature, 439, 45, doi: 10.1038/nature04364

Gabici, S., Evoli, C., Gaggero, D., et al. 2019, Int. J. Mod. Phys. D, 28, 1930022, doi: 10.1142/S0218271819300222

Gaensler, B. M., & Slane, P. O. 2006, Ann. Rev. Astron. Astrophys., 44, 17, doi: 10.1146/annurev.astro.44.051905.092528

Giacinti, G., Mitchell, A. M. W., López-Coto, R., et al. 2020, Astron. Astrophys., 636, A113, doi: 10.1051/0004-6361/201936505

Linden, T., & Buckman, B. J. 2018, Phys. Rev. Lett., 120, 121101, doi: 10.1103/PhysRevLett.120.121101

Lorimer, D. R., Faulkner, A. J., Lyne, A. G., et al. 2006, Mon. Not. Roy. Astron. Soc., 372, 777, doi: 10.1111/j.1365-2966.2006.10887.x

Nava, L., Benyamin, D., Piran, T., & Shaviv, N. J. 2017, Mon. Not. Roy. Astron. Soc., 466, 3674, doi: 10.1093/mnras/stw3346

Peron, G., Aharonian, F., Casanova, S., Yang, R., & Zanin, R. 2021, Astrophys. J. Lett., 907, L11, doi: 10.3847/2041-8213/abcaa9

Pothast, M., Gaggero, D., Storm, E., & Weniger, C. 2018, JCAP, 10, 045, doi: 10.1088/1475-7516/2018/10/045

Recchia, S., Blasi, P., & Morlino, G. 2016, Mon. Not. Roy. Astron. Soc., 462, L88, doi: 10.1093/mnrasl/slw136

Steppa, C., & Egberts, K. 2020, Astron. Astrophys., 643, A137, doi: 10.1051/0004-6361/202038172

Strong, A. W. 2007, Astrophys. Space Sci., 309, 35, doi: 10.1007/s10509-007-9480-1

Sudoh, T., Linden, T., & Beacom, J. F. 2019, Phys. Rev. D, 100, 043016, doi: 10.1103/PhysRevD.100.043016

Sudoh, T., Linden, T., & Hooper, D. 2021. https://arxiv.org/abs/2101.11026

Torres, D. F., Cillis, A., Martín, J., & de Oña Wilhelmi, E. 2014, JHEAp, 1-2, 31, doi: 10.1016/j.jheap.2014.02.001

Weekes, T., Badran, H., Biller, S., et al. 2002, Astropart. Phys., 17, 221, doi: 10.1016/S0927-6505(01)00152-9

Yang, R., Aharonian, F., & Evoli, C. 2016, Phys. Rev. D, 93, 123007, doi: 10.1103/PhysRevD.93.123007

APPENDIX

A. SUPPLEMENTARY MATERIALS

In this section, we give the results obtained by considering $\alpha = 1.5$ for the source luminosity distribution. In Tab.3, we report the resolved ($\Phi^{\rm R}_{\rm GeV}$) and unresolved ($\Phi^{\rm NR}_{\rm GeV}$) fluxes produced by PWNe at different distances from the Galactic center. In Fig.4, we show the spectral behaviour of unresolved PWNe contribution.

In Tab.4, we give the spectral index of CR diffuse emission inferred by fitting Fermi-LAT data with (Γ_{BF}) and without (Γ_1) PWNe contribution. We see that non-negligible effects are obtained in the rings closer to the Galactic center. The predicted emission from PWNe is, however, smaller than what obtained for $\alpha = 1.8$. Correspondingly, a smaller variation $\Delta\Gamma = \Gamma_{BF} - \Gamma_1 \simeq 0.08$ is obtained in the inner Galaxy that partially accounts for the spectral anomaly observed by Fermi-LAT.

Table 3. *Same as Tab.1 for* $\alpha = 1.5$

	$\Phi^{\rm NR}_{\rm GeV}$ $(cm^{-2}\ s^{-1})$		$\Phi^{\rm R}_{\rm GeV}$ $(cm^{-2}\ s^{-1})$	
	$R_\Phi = 500$	$R_\Phi = 1000$	$R_\Phi = 500$	$R_\Phi = 1000$
$1.7 - 4.5$ kpc	3.37×10^{-8} (8.7%)	4.76×10^{-8} (12.3%)	3.41×10^{-8}	8.8×10^{-8}
$4.5 - 5.5$ kpc	1.75×10^{-8} (5.6%)	2.47×10^{-8} (7.9%)	2.50×10^{-8}	6.04×10^{-8}
$5.5 - 6.5$ kpc	1.76×10^{-8} (3.4%)	2.48×10^{-8} (4.9%)	3.47×10^{-8}	7.97×10^{-8}
$6.5 - 7.0$ kpc	8.31×10^{-9} (3.2%)	1.17×10^{-8} (4.5%)	2.31×10^{-8}	5.12×10^{-8}
$7.0 - 8.0$ kpc	1.58×10^{-8} (2.0%)	2.24×10^{-8} (2.9%)	7.29×10^{-8}	1.55×10^{-7}
$8.0 - 10.0$ kpc	2.27×10^{-8} (0.6%)	3.25×10^{-8} (0.8%)	2.08×10^{-7}	4.3×10^{-7}
$10.0 - 16.5$ kpc	1.35×10^{-8} (1.8%)	2.00×10^{-8} (2.6%)	2.18×10^{-8}	5.06×10^{-8}
$16.5 - 50.0$ kpc	5.23×10^{-10} (2.1%)	8.37×10^{-10} (1.9%)	1.00×10^{-10}	4.1×10^{-10}
$0.0 - 50.0$ kpc	1.32×10^{-7}(1.9%)	1.88×10^{-7} (2.7%)	4.22×10^{-7}	9.22×10^{-7}

Table 4. *Same as Tab.2 for* $\alpha = 1.5$

Ring	Γ_1	Γ_{BF}	$\alpha = 1.5$
		$R_\Phi = 500$	$R_\Phi = 1000$
$1.7 - 4.5$ kpc	2.56 ± 0.02	2.64 ± 0.01	2.62 ± 0.01
$4.5 - 5.5$ kpc	2.48 ± 0.02	2.52 ± 0.01	2.51 ± 0.01
$5.5 - 6.5$ kpc	2.54 ± 0.04	2.58 ± 0.01	2.57 ± 0.01
$6.5 - 7$ kpc	2.54 ± 0.01	2.57 ± 0.01	2.56 ± 0.01
$7 - 8$ kpc	2.57 ± 0.01	2.583 ± 0.008	2.572 ± 0.008
$8 - 10$ kpc	2.642 ± 0.003	2.642 ± 0.003	2.644 ± 0.004
$10 - 16.5$ kpc	2.696 ± 0.008	2.724 ± 0.008	2.712 ± 0.008
$16.5 - 50$ kpc	2.72 ± 0.03	2.75 ± 0.04	2.74 ± 0.03

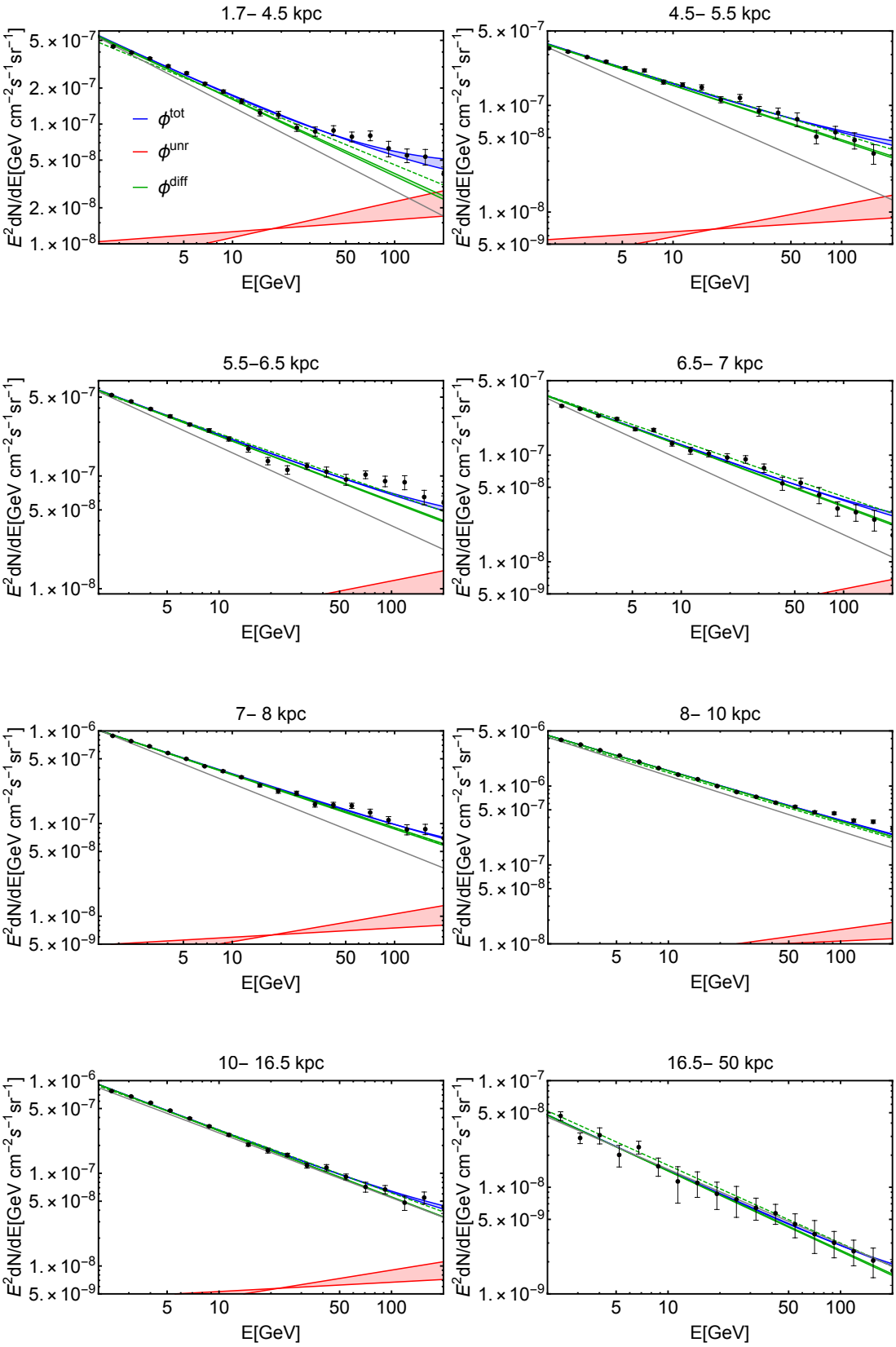

Figure 4. *Color code as in Fig.1 for* $\alpha = 1.5$.